Acta Crystallographica Section D
Biological Crystallography
ISSN 0907-4449

Structures of oncogenic, suppressor and rescued p53 core-domain variants: mechanisms of mutant p53 rescue

Brad D. Wallentine,[a]‡ Ying Wang,[a]‡ Vira Tretyachenko-Ladokhina,[a] Martha Tan,[a] Donald F. Senear[a] and Hartmut Luecke[a,b,c,d,e]*

[a]Department of Molecular Biology and Biochemistry, University of California, Irvine, Irvine, CA 92697, USA, [b]Department of Physiology and Biophysics, University of California, Irvine, Irvine, CA 92697, USA, [c]Department of Computer Science, University of California, Irvine, Irvine, CA 92697, USA, [d]Center for Biomembrane Systems, University of California, Irvine, Irvine, CA 92697, USA, and [e]Unidad de Biofisica (CSIC, UPV/EHU) and Departamento de Bioquimica, Universidad del Pais Vasco, 48940 Leioa, Spain

‡ These authors contributed equally.

Correspondence e-mail: hudel@uci.edu

Received 22 May 2013
Accepted 25 July 2013

PDB References: p53, V157F mutant, 4kvp; N235K mutant, 4lo9; N239Y mutant, 4loe; V157F/N235K/N239Y mutant, 4lof

To gain insights into the mechanisms by which certain second-site suppressor mutations rescue the function of a significant number of cancer mutations of the tumor suppressor protein p53, X-ray crystallographic structures of four p53 core-domain variants were determined. These include an oncogenic mutant, V157F, two single-site suppressor mutants, N235K and N239Y, and the rescued cancer mutant V157F/N235K/N239Y. The V157F mutation substitutes a smaller hydrophobic valine with a larger hydrophobic phenylalanine within strand S4 of the hydrophobic core. The structure of this cancer mutant shows no gross structural changes in the overall fold of the p53 core domain, only minor rearrangements of side chains within the hydrophobic core of the protein. Based on biochemical analysis, these small local perturbations induce instability in the protein, increasing the free energy by 3.6 kcal mol^{-1} (15.1 kJ mol^{-1}). Further biochemical evidence shows that each suppressor mutation, N235K or N239Y, acts individually to restore thermodynamic stability to V157F and that both together are more effective than either alone. All rescued mutants were found to have wild-type DNA-binding activity when assessed at a permissive temperature, thus pointing to thermodynamic stability as the critical underlying variable. Interestingly, thermodynamic analysis shows that while N239Y demonstrates stabilization of the wild-type p53 core domain, N235K does not. These observations suggest distinct structural mechanisms of rescue. A new salt bridge between Lys235 and Glu198, found in both the N235K and rescued cancer mutant structures, suggests a rescue mechanism that relies on stabilizing the β-sandwich scaffold. On the other hand, the substitution N239Y creates an advantageous hydrophobic contact between the aromatic ring of this tyrosine and the adjacent Leu137. Surprisingly, the rescued cancer mutant shows much larger structural deviations than the cancer mutant alone when compared with wild-type p53. These suppressor mutations appear to rescue p53 function by creating novel intradomain interactions that stabilize the core domain, allowing compensation for the destabilizing V157F mutation.

1. Introduction

The tumor suppressor protein p53 functions as a transcription factor to stimulate cell-cycle arrest, DNA repair or apoptosis in response to a variety of cellular stress signals (Bullock & Fersht, 2001; Vogelstein *et al.*, 2000; Römer *et al.*, 2006; Riley *et al.*, 2008; Kruse & Gu, 2009). In addition to a DNA-binding core domain, p53 contains an N-terminal transactivation domain, a tetramerization domain and a basic C-terminal

domain (Joerger & Fersht, 2008). The core domain consists of a β-sandwich scaffold which defines the DNA-binding surface (Cho *et al.*, 1994). Mutations in the p53 tumor suppressor gene lead to loss of its normal function, giving rise to a higher oncogenic potential for the cell. Statistical analysis shows that about half of all human tumors carry mutant *p53* alleles, about 70% of which are single-site missense mutations located in the core domain (IARC TP53 Database, version R16; http://p53.iarc.fr; Vousden & Lu, 2002; Petitjean *et al.*, 2007). There are three core-domain missense mutation phenotypes, which are classified predominantly by their thermodynamic and DNA-binding properties (Bullock *et al.*, 1997, 2000). The first category is comprised of mutations that affect direct DNA-contact amino acids. Mutations in the second category have distorted local structural elements but maintain native-like thermodynamic properties. Mutations in the third category lead to thermodynamically destabilized proteins that are globally unfolded at 310 K. This third class includes most mutations in the β-sandwich region studied to date. β-Sandwich mutations account for approximately 28% of all p53 cancer mutations and their rescue is the focus of research interest here (Brachmann, 2004).

Considerable efforts are being undertaken to design pharmaceuticals that can restore normal cellular functions to these mutated p53 proteins. To understand how these pharmaceuticals could be designed, researchers began by using a systematic genetic approach. This approach screens for novel point mutations in the p53 gene, known as second-site suppressor mutations or rescue mutations, which restore wild-type function to a previously nonfunctional p53 mutant (Brachmann *et al.*, 1998). In correspondence with the three categories of cancer mutations, three rationally designed suppressor mutation classes have emerged: (i) mutations that provide additional contacts to bind DNA; (ii) mutations that compensate local structural disruptions; and (iii) mutations that stabilize the overall core-domain structure. An example of the first class of suppressor mutations is T284R, which restores native-like DNA-binding affinity to DNA-contact mutants R273C and R273H by providing a new DNA contact (Wieczorek *et al.*, 1996). The second category is illustrated by the structure of the H168R/R249S mutant. It reveals a mechanism whereby the introduction of a guanidinium *via* Arg168 mimics the function of Arg249 which is lost in the R249S cancer mutant, thereby limiting the structural distortion of the DNA-binding surface (Joerger *et al.*, 2005). However, owing to the large number of cancer mutations, screening for specific suppressor variants to correct the defect caused by each cancer mutant individually appears to be impractical. Stabilizing second-site suppressor mutations in the third class hold the promise of more broadly effective rescue mechanisms, with a single second-site suppressor mutation able to rescue the effects of several destabilizing missense mutations. Second-site suppressor mutations known to rescue multiple oncogenic mutations are known as global suppressor mutations.

With the reliance on second-site suppressor mutations to design pharmaceuticals that can restore function to a variety of p53 mutants, understanding global suppressor mutations has become particularly lucrative. Specific mutations at positions 235, 239 and 240 have been identified from such screens as potential global suppressors (Baroni *et al.*, 2004). These mutations, alone or in combination, are capable of restoring function to 13 of 30 of the most common p53 cancer mutants (Baroni *et al.*, 2004; Brachmann, 2004; Brachmann *et al.*, 1998). Substitutions at two positions, Lys235 and Tyr239, are particularly effective in restoring function to β-sandwich cancer mutants. In combination with other second-site suppressor mutations, N235K is able to restore function to six of the seven most common β-sandwich mutants studied (Baroni *et al.*, 2004). N239Y is able to rescue three of these seven β-sandwich mutations when acting alone and five when combined with other second-site suppressor mutations (Baroni *et al.*, 2004). Because most β-sandwich mutations belong to the destabilizing category of cancer mutants studied to date, it is expected that both N235K and N239Y may enhance the thermodynamic stability of the p53 core domain. Indeed, previous thermodynamic studies have revealed that N239Y enhances stability by more than 1 kcal mol^{-1} (4.184 kJ mol^{-1}; Wang *et al.*, 2003; Nikolova *et al.*, 1998).

Currently, no crystal structure of a β-sandwich mutant exists without additional stabilizing mutations. It is important to study the structural effects of these β-sandwich mutations and how they lead to instability of the core domain. Additionally, no literature has addressed the structural basis of the N235K rescue mechanism. The structural effects of the N239Y suppressor mutation have previously been studied in the context of the M133L/V203A/N239Y/N268D mutant (PDB entry 1uol), referred to as the thermostable mutant or T-p53 in the following text, which forms a hyper-stable core (Joerger *et al.*, 2004). It is interesting to examine the individual structural effects of N239Y independently from the other three mutations of this thermostable mutant.

These considerations motivated our analysis of the oncogenic mutation V157F and the rescue mechanisms of N235K and N239Y. To this end, we have conducted thermodynamic and biochemical analyses of the oncogenic V157F mutant, one of the most strongly destabilized β-sandwich cancer mutants; the second-site suppressor mutants N235K and N239Y; and the rescue of V157F by N235K/N239Y. We found that N235K is an effective stabilizer of V157F, despite having almost no effect on the thermodynamic stability of the wild-type p53 core domain. N239Y stabilizes both V157F and wild-type p53 to a similar degree. Furthermore, we determined and analyzed the crystal structures of four p53 variants: the oncogenic mutant V157F, the two suppressor mutants N235K and N239Y, and the oncogenic mutant in conjunction with both suppressor mutations, V157F/N235K/N239Y, referred to as the rescued cancer mutant in the following text. By comparing these mutant structures with that of wild-type p53 (Wang *et al.*, 2007; Cho *et al.*, 1994), we find that both of these suppressor mutations create novel residue interactions that stabilize the native p53 structure (Wang *et al.*, 2007; Cho *et al.*, 1994). These findings enhance our understanding of global suppressor motifs and afford valuable knowledge as p53 rescue is

Table 1
Data-collection and refinement statistics.

Values in parentheses are for the outer resolution shell.

	V157F	N235K	N239Y	V157F/N235K/N239Y
Data collection and processing				
Space group	$P2_1$	$P2_1$	$P2_1$	$P2_12_12$
Unit-cell parameters				
a (Å)	68.7	69.2	68.9	107.3
b (Å)	70.3	69.2	71.1	51.1
c (Å)	83.6	83.9	84.3	33.8
α (°)	90.0	90.0	90.0	90.0
β (°)	90.1	90.1	90.1	90.0
γ (°)	90.0	90.0	90.0	90.0
Monomers per asymmetric unit	4	4	4	1
Resolution range (Å)	42.35–1.50 (1.53–1.50)	53.38–2.50 (2.59–2.50)	29.11–1.85 (1.91–1.85)	46.15–2.00 (2.07–2.00)
Observed reflections	409378	98333	245716	60576
Unique reflections	122789	27431	68899	12822
Completeness (%)	96.6 (94.1)	99.2 (96.6)	98.35 (92.0)	97.3 (99.3)
$\langle I/\sigma(I)\rangle$	8.2 (2.6)	8.0 (3.5)	8.6 (2.6)	5.8 (2.6)
Multiplicity	3.33 (3.01)	3.58 (3.38)	3.57 (3.56)	4.7 (4.8)
$R_{\rm merge}$† (%)	7.1 (31.3)	10.7 (28.6)	8.4 (46.9)	16.9 (47.7)
Refinement				
Protein atoms	6118	6096	6135	1564
Protein residues	777	776	776	198
Zinc ions	4	4	4	1
Water molecules	536	252	534	134
Resolution range (Å)	42.35–1.50	53.38–2.50	29.11–1.85	46.15–2.00
Twin ratio (%)	88/12	N/A	N/A	N/A
R‡ (%)	17.6	18.1	18.8	19.6
$R_{\rm free}$§ (%)/% of the test set	21.0/7.3	24.7/7.3	24.4/2.9	25.6/8.0
R.m.s.d., bond lengths¶ (Å)	0.005	0.009	0.007	0.008
R.m.s.d., bond angles¶ (°)	1.0	1.2	1.1	1.1
Ramachandran plot, residues in (%)				
Core regions (%)	99.6	99.0	99.2	98.0
Additional allowed regions (%)	0.4	0.7	0.8	2.0
Generously allowed regions (%)	0.0	0.4	0.0	0.0
Disallowed regions (%)	0.0	0.0	0.0	0.0

† $R_{\rm merge} = \sum_{hkl}\sum_i |I_i(hkl) - \langle I(hkl)\rangle| / \sum_{hkl}\sum_i I_i(hkl)$, where $I_i(hkl)$ is the mean intensity of symmetry-related reflections. ‡ $R = \sum_{hkl} ||F_{\rm obs}| - |F_{\rm calc}|| / \sum_{hkl} |F_{\rm obs}|$, where $|F_{\rm obs}|$ and $|F_{\rm calc}|$ are the observed and calculated structure-factor amplitudes, respectively. § $R_{\rm free}$ is calculated using part of the data that was withheld from refinement. ¶ Root-mean-square deviation.

beginning to move towards providing clinical value (Lehmann *et al.*, 2012).

2. Materials and methods

2.1. Protein purification and crystallization

The DNA sequences encoding the human p53 core-domain (residues 94–312) mutants V157F, N235K, N239Y and V157F/N235K/N239Y were subcloned into the pSE420 (Invitrogen) bacterial expression vector. The plasmids were transformed into the *Escherichia coli* BL21 (DE3) strain. Cells were initially grown at 303 K to an OD_{600} of 1.2 before overnight induction with 0.5 m*M* IPTG (isopropyl β-D-1-thiogalactopyranoside) and 1 m*M* zinc sulfate at 283 K. The cells were isolated by centrifugation and sonicated in 50 m*M* imidazole pH 7.2, 5 m*M* dithiothreitol (DTT) with protease-inhibitor cocktail tablets (Roche). The supernatant was loaded onto a SP Sepharose cation-exchange column (Pharmacia) and eluted with an NaCl gradient (0–600 m*M*). Elution fractions were diluted in 5–6 volumes of buffer with 50 m*M* imidazole pH 7.2, 5 m*M* DTT and 50 m*M* NaCl. Further purification was achieved by affinity chromatography using a HiTrap Heparin Sepharose column in 50 m*M* imidazole pH 7.2, 5 m*M* DTT with an NaCl gradient (0–600 m*M*). Elution fractions were dialyzed against 20 m*M* Tris pH 7.6, 150 m*M* NaCl, 10 m*M* DTT. The columns were kept at 277 K. The mutant proteins were concentrated to 15 mg ml^{-1} and stored at 253 K until further use. Crystals were grown at 277 K using the sitting-drop or hanging-drop vapour-diffusion technique. 2 µl protein solution (∼5.0–7.0 mg ml^{-1} protein in 20 m*M* Tris pH 7.6, 150 m*M* NaCl, 10 m*M* DTT) was mixed with 2 µl reservoir buffer. The reservoir conditions were different for the individual mutants as follows: 25%(*w*/*v*) polyethylene glycol (PEG) 2000 monomethyl ether (MME) for the V157F mutant, 100 m*M* HEPES, 30%(*w*/*v*) polyethylene glycol (PEG) 6000 pH 7.0 for the N235K mutant, 200 m*M* lithium acetate, 20%(*w*/*v*) PEG 3350 for the N239Y mutant and 200 m*M* disodium hydrogen phosphate dehydrate (Na_2HPO_4), 20%(*w*/*v*) PEG 3350 for the V157F/N235K/N239Y mutant. Colorless plate-shaped crystals were obtained within a week. The crystals were flash-cooled in cryobuffer with 40%(*w*/*v*) PEG 2000 MME (monomethyl ether) for the V157F crystals, 35%(*w*/*v*) PEG 6000 for the N235K crystals and 35%(*w*/*v*) PEG 3350 for the N239Y and V157F/N235K/N239Y crystals.

2.2. Data collection and structure determination

Diffraction data sets for the N235K and V157F/N235K/N239Y crystals were collected at 100 K on beamline 4.2.2 at the Advanced Light Source (ALS) in Berkeley, while diffraction data sets for the V157F and N239Y crystals were collected at 100 K on beamlines 9-1 and 1-5 at Stanford Synchrotron Radiation Laboratory (SSRL). The data sets were indexed, integrated and further processed using the program *d*TREK* (Pflugrath, 1999). Data-collection statistics are summarized in Table 1.

Since the V157F, N235K and N239Y crystals were isomorphous to our wild-type p53 crystals, with very similar unit-cell parameters, all four molecules in the asymmetric unit of the wild-type p53 were used as the primary model for rigid-body refinement in *CNS* (Brünger *et al.*, 1998; Wang *et al.*, 2007). The V157F/N235K/N239Y mutant crystallized in a different space group ($P2_12_12$) and molecular replacement was carried

Table 2
Equilibrium characteristics of p53 cancer, suppressor and rescued cancer mutants.

	Folding stability							
	Fitted parameters			Calculated parameters†		DNA binding		
p53 variant	m† (kcal mol^{-1} M^{-1})	[Urea]$_{0.5}$ (kcal mol^{-1})	s‡	$\Delta G_{D-N}^{H_2O}$ (kcal mol^{-1})	$\Delta\Delta G_{D-N}$ (kcal mol^{-1})	ΔG_{spec} (kcal mol^{-1})	$\Delta G_{non\text{-}spec}$ (kcal mol^{-1})	s‡
N239Y	3.50 ± 0.29	3.33 ± 0.02	0.028	−10.4 ± 0.07	−0.88	−7.95 ± 0.056	−6.86 ± 0.008	0.082
N235K	2.61 ± 0.11	3.11 ± 0.01	0.021	−9.7 ± 0.06	−0.19	−7.66 ± 0.022	−7.03 ± 0.044	0.035
Wild type	3.35 ± 0.19	3.00 ± 0.02	0.018	−9.5 ± 0.07	—	−8.00 ± 0.021	−7.02 ± 0.021	0.035
V157F/N235K/N239Y	3.00 ± 0.20	2.61 ± 0.01	0.030	−8.2 ± 0.06	1.36	−7.99 ± 0.040	−7.04 ± 0.085	0.078
V157F/N235K	2.70 ± 0.17	2.32 ± 0.02	0.028	−7.2 ± 0.07	2.28	−8.14 ± 0.019	−7.21 ± 0.064	0.037
V157F	3.31 ± 0.42	1.90 ± 0.03	0.050	−5.9 ± 0.08	3.60	nd§	nd§	

† The weighted mean value of m for these six urea-denaturation transitions is 2.97 ± 0.14 kcal mol^{-1} M^{-1}, which is indistinguishable from the value of 3.12 ± 0.05 kcal mol^{-1} M^{-1} reported previously (Bullock *et al.*, 2000; Nikolova *et al.*, 2000). In consideration of the much larger number of p53 variants represented in the earlier value and to facilitate comparison, we have used m = 3.12 kcal mol^{-1} M^{-1} to calculate $\Delta G_{D-N}^{H_2O}$ and $\Delta\Delta G_{D-N}$ from (2) in the text. ‡ Square root of the variance of the fitted curve. The parameters from the fits to (1) were used to transform s from the fitted units of intensity to the fraction unfolded, as plotted in Fig. 1. § Not determined. The low thermal stability of this mutant precluded these measurements.

out with the program *Phaser* using molecule *A* of the DNA-free wild-type p53 core domain as the search model (Storoni *et al.*, 2004; Wang *et al.*, 2007). All models were manually rebuilt into $2F_o - F_c$ and $F_o - F_c$ maps using the programs *O* and/or *Coot* (Jones *et al.*, 1991; Emsley & Cowtan, 2004). Diffraction data were checked for twinning using *POINTLESS* and *phenix.triage* (Evans, 2006; Adams *et al.*, 2010). No twinning was indicated for the N235K, N239Y or V157F/N235K/N239Y crystals. The V157F crystal contained a twinned fraction of 0.12 with twinning operation h, $-k$, $-l$. Subsequent refinement was carried out in *CNS* and *PHENIX*, with an h, $-k$, $-l$ twin target used during refinement of V157F with *PHENIX* (Brünger *et al.*, 1998; Adams *et al.*, 2010; Afonine *et al.*, 2012). Water molecules were added to the structures using the waterpick option implemented in *CNS* and the Update Waters option in *PHENIX* (Brünger *et al.*, 1998; Afonine *et al.*, 2012). The stereochemistry of the models was validated with *PROCHECK* or *MolProbity* and all four p53 mutant structures had excellent stereochemistry (Laskowski *et al.*, 1996; Chen *et al.*, 2010). Details of the model refinement are presented in Table 1.

Figures were generated with *PyMOL* (DeLano, 2002). Pairwise alignment of p53 structures for root-mean-square deviations was performed using the secondary-structure matching function within *Coot* (Krissinel & Henrick, 2004).

2.3. Protein Data Bank accession codes

The atomic coordinates and structure factors for the cancer mutant (V157F), the suppressor mutants (N235K and N239Y) and the rescued cancer mutant (V157F/N235K/N239Y) have been deposited in the RCSB Protein Data Bank under accession codes 4kvp, 4lo9, 4loe and 4lof, respectively.

2.4. Solute denaturation

Equilibrium unfolding of the p53 core domain was monitored by intrinsic protein fluorescence as described by Bullock *et al.* (1997). Individual p53 mutant samples in 50 m*M* sodium phosphate buffer pH 7.2 containing 5 m*M* DTT plus urea at concentrations ranging from 0 to 5.5 *M* were incubated overnight at 283 K. Fluorescence emission spectra (an average of 20 scans) were recorded from 300 to 370 nm using an SLM-8100 spectrofluorometer in 2 × 10 mm cuvettes in a Peltier-controlled cell holder at 283 K. Excitation was at 280 nm and the bandpass was 8 nm on both excitation and emission. Folded p53 core domain generates a characteristic emission spectrum with a peak at 305 nm reflecting strong contributions from some or all of the eight tyrosine residues of the protein. A long tail extending to the red reflects a weak contribution from its single tryptophan residue, which is probably quenched. Unfolded monomeric p53 is characterized by a decrease in emission at 305 nm and the appearance of a peak at around 350 nm, consistent with decreased tyrosine emission and increased tryptophan emission. An isofluorescence point at about 320 nm is indicative of a two-state unfolding transition. These data are consistent with data published previously (Bullock *et al.*, 1997).

Baseline-subtracted spectra were normalized using the isofluorescence for all variants except V157F. Aggregated p53 is characterized by broad emission with a maximum near 340 nm (Bullock *et al.*, 2000). A small amount of this material that was present in V157F samples precluded normalization. The difference in intensity, $I_{356} - I_{305}$, was fitted as a function of urea concentration to (1), which assumes a two-state unfolding model and a linear dependence of the fluorescence for both the folded and unfolded states on urea concentration (Pace, 1986),

$$I_{obs} = (I_N + m_N[\text{urea}]) + (I_D + m_D[\text{urea}]) \times \frac{\exp\{-m_{urea}([\text{urea}] - [\text{urea}]_{0.5})/RT\}}{1 + \exp\{-m_{urea}([\text{urea}] - [\text{urea}]_{0.5})/RT\}}, \quad (1)$$

where $I_{obs} = I_{356} - I_{305}$ and I_N and I_U represent the intercepts and m_N and m_U represent the slopes of the pre-unfolding (native protein) and post-unfolding (unfolded protein) baselines. [Urea]$_{0.5}$ is the midpoint of the transition and m_D is the slope of the linear dependence of the unfolding free energy (ΔG_{D-N}) on the urea concentration. Data were fitted using the program *Origin* 7.0. Independent urea denaturations of a large number or p53 variants by others and by us (Table 2) have yielded very similar values of m_{urea}, suggesting that this parameter is little affected by mutation (Bullock *et al.*, 1997,

2000; Nikolova *et al.*, 1998, 2000). Given a linear dependence of $\Delta G_{\mathrm{D-N}}$ on urea concentration, the folding stability in the absence of denaturant is approximated well by

$$\Delta G_{\mathrm{D-N}}^{\mathrm{H_2O}} = \langle m_{\mathrm{urea}} \rangle \cdot [\mathrm{urea}]_{0.5}, \quad (2)$$

where $\langle m_{\mathrm{urea}} \rangle$ is the average of independently determined values.

2.5. DNA binding

Site-specific binding of p53 variants was analyzed using the electrophoretic mobility-shift assay (EMSA). The DNA-binding target used was a 30-base-pair double-stranded oligonucleotide containing the native sequence surrounding the p53 binding site at the *gadd45* promoter. The top strand (5′-GTACAGAACATGTCTAAGCATGCTGGGGAC-3′) conjugated at its 5′ end to Oregon Green 514 *via* a 6-carbon linker and complementary bottom-strand oligonucleotides were purchased from Integrated DNA Technologies Inc. (Coralville, Iowa, USA). These were annealed to double strand as described previously (Tretyachenko-Ladokhina *et al.*, 2006). Reaction mixtures (20 µl) containing 50 n*M* *gadd45* DNA and p53 ranging in concentration from 0.05 to 10 µ*M* in 10 m*M* PIPES pH 6.8, 100 m*M* NaCl, 5 m*M* DTT, 1%(*w*/*v*) Ficoll 400 were incubated for 20 min in a water bath at 283 K. Bound and free *gadd45* species were separated by electrophoresis on 5% acrylamide TBE mini-gels (either pre-cast Readygels with 29:1 acrylamide:bis-acrylamide or hand-cast gels with 39:1 acrylamide:bis-acrylamide). Gels were pre-electrophoresed for 6 min at a constant 200 V (∼10 mA per gel) prior to loading the samples with the current on at reduced voltage (25 V). Electrophoresis was at a constant 100 V (∼11 mA per gel) for 40 min.

The wet gels were imaged using a GE Healthcare Typhoon 9400. Excitation and emission used a 488 nm laser and a 520 nm 40 nm bandpass filter, respectively. The images were analyzed as described previously to determine the fraction of DNA (θ_{i}) in each of the electrophoretic bands (Senear & Brenowitz, 1991). Unliganded *gadd45* DNA and the specific complex (first mobility-shifted band) were analyzed individually. A short ladder of lower mobility bands corresponding to higher order species that presumably represent additional nonspecific interactions was poorly resolved. These were grouped together to yield θ_{N}. The fractions of these species are given as a function of the p53 concentration by

$$\theta_i = \frac{\exp(i \cdot \ln[\mathrm{p53}] - \Delta G_i/RT)}{\sum_i \exp(i \cdot \ln[\mathrm{p53}] - \Delta G_i/RT)}, \quad (3)$$

where i is the p53 stoichiometry in each of the complexes and ΔG_i is the free-energy change per monomer for binding to form the particular complex. For the specific complex, i was set equal to 4 to account for concerted binding of the p53 monomer to form tetramer-bound p53 (McLure & Lee, 1998). The value of i was adjusted for the higher order complexes (θ_{N}). The best fit was obtained with $i = 6$, indicating that a hexamer is the average stoichiometry of these higher order species. Thus, the summation in the denominator of (3) is over $i = 0$, 4 and 6.

3. Results

3.1. Equilibrium properties of p53 cancer, rescued and suppressor mutants

As a first step to delineate the rescue mechanism mediated by the suppressor mutations N235K and N239Y, we conducted a thermodynamic analysis of their rescue of the V157F cancer mutation. Although it is one of the most strongly destabilized β-sandwich p53 cancer mutants, in yeast assays the wild-type function of the V157F mutant is restored by either N235K or N239Y alone as well as both together (Baroni *et al.*, 2004; Danziger *et al.*, 2007). Stability was assessed using urea-induced unfolding at 283 K, a permissive temperature at which even severely destabilized cancer mutants such as V157F are predominantly folded (Bullock *et al.*, 2000).

Unfolding titrations for the wild-type core domain, the cancer mutant, both suppressor mutants and two rescued cancer mutants are shown in Fig. 1. The parameters obtained by analysis of these data using (1) as described below are listed in Table 2. The urea concentration at the midpoints of the unfolding transitions varies substantially from 3.3 to 1.9 *M*, indicating widely varying stability. However, the slopes of the transitions, obtained independently, do not vary. This feature is in accord with all previous reports and the weighted mean value of the slope obtained from these six p53 variants, 2.97 ± 0.14 kcal mol^{-1} *M*$^{-1}$, is in the middle of the range of previous reports (Bullock *et al.*, 1997, 2000; Nikolova *et al.*, 1998, 2000). Based on this, we have used the average slope to calculate

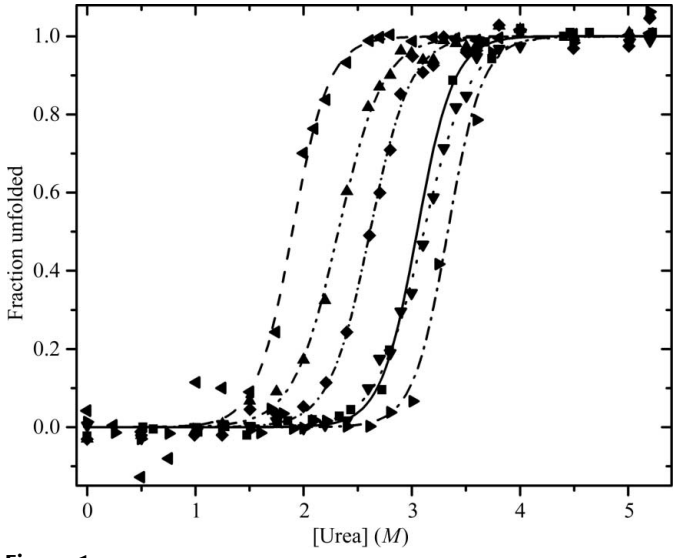

Figure 1
Urea-induced denaturation of wild-type and mutant p53 core domains at 283 K. The unfolding of wild-type p53 (squares) and the V157F (triangles pointing left), N235K (triangles pointing down), N239Y (triangles pointing right), V157F/N235K (triangles pointing up) and V157F/N235K/N239Y (diamonds) mutants was monitored by the difference in fluorescence intensity as described in the text. The curves indicate the fits to (1). The data plotted have been transformed from fluorescence to fraction unfolded.

the free-energy change for folding in the absence of urea ($\Delta G_{D-N}^{H_2O}$) and the difference for each variant compared with the wild-type p53 core domain ($\Delta\Delta G_{D-N}$).

The results that we obtained for wild-type p53, −9.5 kcal mol^{-1}, and for the V157F cancer mutant, −5.9 kcal mol^{-1}, are indistinguishable from those reported previously (Bullock *et al.*, 2000). The results for N239Y are also similar to those reported previously, although we find a somewhat smaller net stabilization of −0.9 kcal mol^{-1} *versus* either −1.2 or −1.5 kcal mol^{-1} (Nikolova *et al.*, 1998, 2000). Perhaps more significantly, the net stabilization is the same whether the N239Y suppressor mutation is introduced into the V157F/N235K variant or whether it is introduced into the wild-type core domain, which is consistent with previous reports of additive effects. In contrast to this behavior, the N235K suppressor mutation yields a negligible net stabilization of the wild-type p53 core domain, whereas this substitution results in robust stabilization of the cancer mutant V157F (−1.32 kcal mol^{-1}; Table 2). Together, N239Y and N235K reduce the destabilization of V157F to only 1.36 kcal mol^{-1}, which is well below the threshold associated with loss of function (Bullock *et al.*, 2000).

Binding of each of the p53 variants to its specific site in the *gadd45* promoter was assayed to assess the functional properties of each of the folded structures. Typical results of these experiments are presented for the N235K suppressor mutant (Fig. 2). The gel image in the inset documents the formation of a prominent mobility-shifted band as a function of p53 concentration, followed by a short ladder of lower mobility bands. Full-length p53 is tetrameric, and the tetramer is the basic DNA-binding unit (McLure & Lee, 1998; Melero *et al.*, 2011; Aramayo *et al.*, 2011). Similarly, the p53 core domain,

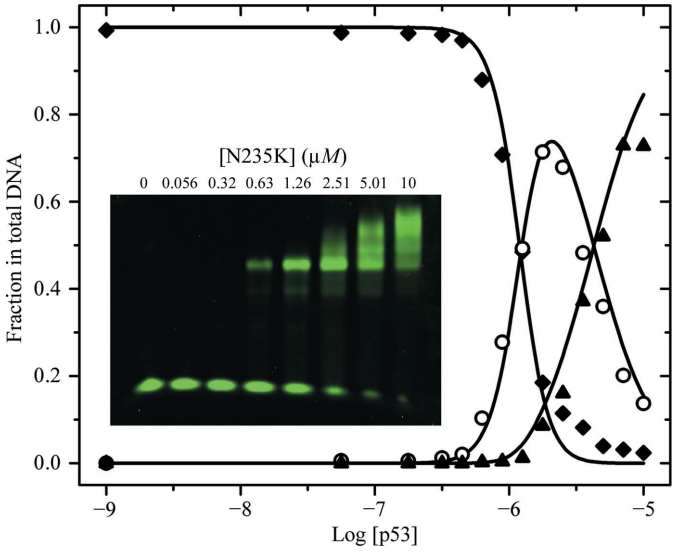

Figure 2
Binding of the N235K core domain to *gadd45* DNA. The inset shows a false colour image of Oregon Green 514 fluorescence from one of two acrylamide gels used to separate bound from free DNA species. The concentrations of the N235K samples are indicated for each lane. The plot shows the fractions of the different DNA species. Symbols are filled diamonds, free DNA (bottom band on gel); open circles, specific p53–*gadd45* complex (first mobility-shifted band); filled triangles, higher order species (summed ladder of additional mobility-shifted bands). Solid lines indicate the fit to (3). Free-energy changes (per p53 monomer) for p53 binding to form the specific tetrameric species and to form higher order species are listed in Table 2.

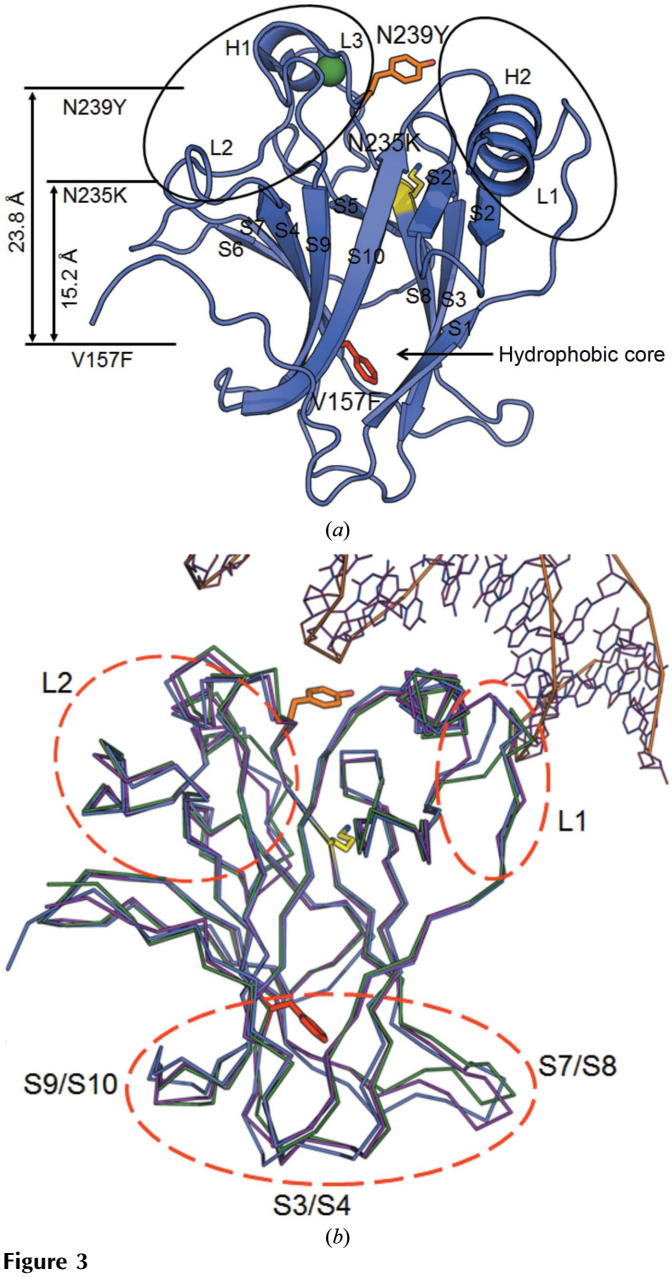

Figure 3
The crystal structure of the rescued cancer mutant V157F/N235K/N239Y (PDB entry 4lof). (*a*) Cartoon representation of the rescued cancer mutant. The β-sandwich scaffold with its hydrophobic core supports the DNA-binding surface, including two large loop regions (circled by two black ellipses). The coordinated zinc ion is highlighted as a green sphere. The oncogenic mutation Phe157 (red) and two suppressor mutations Lys235 (yellow) and Tyr239 (orange) were mapped as stick models in the overall structure. The three mutations are spatially separated as indicated. (*b*) Backbone-atom alignment of the rescued cancer mutant V157F/N235K/N239Y (blue) with DNA-free wild-type p53 (PDB entry 2ocj, chain *B*; green) and DNA-bound wild-type p53 in complex with the consensus DNA (PDB code 1tsr, chain *B*; purple). Dotted red ellipses indicate the regions of significant structural deviations. The cancer mutation Phe157 (red) and two suppressor mutations Lys235 (yellow) and Tyr239 (orange) are mapped as stick models.

Table 3
Pairwise root-mean-square (r.m.s.) deviations (in Å) of different human p53 core-domain structures (values related to the rescued cancer mutant V157F/N235K/N239Y are highlighted in bold).

	1tsr_*B*, DNA-bound	2ocj_*B*, DNA-free	4kvp_*B*, V157F	4lo9_*B*, N235K	4loe_*B* N239Y	4lof, V157F/N235K/N239Y	1uol_*B*, M133L/V203A/N239Y/N268D	2bim_*B*, T-p53c, R273H	2bin, T-p53c, H168R	2bio, T-p53c, R249S	2bip, T-p53c, H168R/R249S	2biq, T-p53c, T123A/H168R/R249S
1tsr_*B*, DNA-bound		0.76	0.76	0.73	0.76	**0.81**	0.71	0.73	0.62	0.75	0.79	0.79
2ocj_*B*, DNA-free	0.76		0.24	0.23	0.20	**0.87**	0.46	0.47	0.50	0.78	0.60	0.56
4kvp_*B*, V157F	0.76	0.24		0.28	0.27	**0.88**	0.46	0.46	0.51	0.82	0.63	0.58
4lo9_*B*, N235K	0.73	0.23	0.28		0.26	**0.86**	0.44	0.46	0.51	0.64	0.62	0.56
4loe_*B* N239Y	0.76	0.20	0.27	0.26		**0.88**	0.46	0.48	0.48	0.75	0.58	0.53
4lof, V157F/N235K/N239Y	**0.81**	**0.87**	**0.88**	**0.86**	**0.88**		**0.74**	**0.77**	**0.82**	**0.89**	**0.95**	**0.90**
1uol_*B*, M133L/V203A/N239Y/N268D	0.71	0.46	0.46	0.44	0.46	**0.74**		0.15	0.45	0.74	0.61	0.53
2bim_*B*, T-p53c, R273H	0.73	0.47	0.46	0.46	0.48	**0.77**	0.15		0.47	0.77	0.61	0.54
2bin, T-p53c, H168R	0.62	0.50	0.51	0.51	0.48	**0.82**	0.45	0.47		0.60	0.38	0.43
2bio, T-p53c, R249S	0.75	0.78	0.82	0.64	0.75	**0.89**	0.74	0.77	0.60		0.70	0.71
2bip, T-p53c, H168R/R249S	0.79	0.60	0.63	0.62	0.58	**0.95**	0.61	0.61	0.38	0.70		0.21
2biq, T-p53c, T123A/H168R/R249S	0.79	0.56	0.58	0.56	0.53	**0.90**	0.53	0.54	0.43	0.71	0.21	

which is monomeric in solution, binds in a cooperative fashion to form a tetramer as the DNA-bound form (Rippin *et al.*, 2002; Weinberg *et al.*, 2004). Consistent with these findings, when the fraction of unbound DNA in our experiments was analyzed as a function of p53 concentration using a Hill model, values of the Hill coefficient ranging from 3 to 3.7 were routinely obtained. Based on this finding, analysis of the specific binding assumed strictly concerted binding of monomers to form DNA-bound tetramers as described in §2. The ladder of lower mobility bands indicates higher order species, which are presumably a consequence of additional electrostatically mediated nonspecific binding as described previously (Weinberg *et al.*, 2004). These bands were combined and analyzed using a single average integral stoichiometry. In all cases, the best fit was obtained with $N = 6$, leading to the binding isotherm (3) described in §2.

The results of the analysis of p53 variants shown in Table 2 indicate a per-subunit free-energy change for binding of -8 kcal mol^{-1} under these conditions, which corresponds to approximately 1 μM affinity. The nonspecific complexes form with an approximately 1 kcal mol^{-1} smaller per-subunit free-energy change. More significant, the DNA-binding properties of all variants, suppressor and rescued cancer studied here are indistinguishable from those of the wild-type p53 core domain at a permissive temperature at which all variants are fully folded.

3.2. Overall structures of p53 mutants

The crystals of the V157F, N235K and N239Y mutants are isomorphous to the DNA-free wild-type p53 crystals (space group $P2_1$; PDB entry 2ocj; Wang *et al.*, 2007). All four molecules in the asymmetric unit are structurally similar, with low root-mean-square (r.m.s.) deviations for the superposition of the backbone atoms. The crystals of the rescued cancer mutant, V157F/N235K/N236Y, formed in a different space group, $P2_12_12$, with one molecule in the asymmetric unit.

Since all mutant crystals were grown at 277 K, a permissive temperature at which all mutants are expected to be fully folded, it is not surprising that the overall fold of these four p53 variants resembles that of the typical wild-type core domain (Fig. 3*a*; Cho *et al.*, 1994; Wang *et al.*, 2007): two twisted antiparallel β-sheets pack together, forming a β-sandwich as a hydrophobic core. Compared with the β-sheet composed of strands S4, S6, S7, S9 and S10, the β-sheet composed of the remaining four strands, S1, S3, S5 and S8, has fewer hydrogen bonds and is more loosely packed. The DNA-binding region includes two large loops, L2 and L3, and a loop–sheet–helix motif comprising loop L1, the S2–S2′ hairpin, the C-terminal residues of strand S10 and helix H2. A zinc ion is bound in a tetrahedrally coordinated complex with the side chains of Cys176, His179, Cys238 and Cys242, stabilizing loops L2 and L3. The cancer mutation Phe157 is located within strand S4 in the hydrophobic core, while the suppressor mutations Lys235 and Tyr239 are in strand S8 and loop L3, respectively. As expected from the evaluation of previous core-domain structures, both suppressor mutations are far from the cancer mutation. The distances between the C$^{\alpha}$ atoms of Phe157 and Lys235 and Tyr239 are 15.2 and 23.8 Å, respectively (Fig. 3*a*). Because of these distances, it is highly unlikely that a direct structural compensation can account for their mechanisms of rescue.

Although no significant perturbation occurs in the overall fold of the p53 mutants, local structural deviations exist among different p53 mutant structures. The r.m.s. deviations between various human p53 core-domain structures are summarized in Table 3. The second column compares the different p53 structures with that of DNA-bound wild-type p53 (PDB entry 1tsr, chain *B*; Cho *et al.*, 1994). In most cases the r.m.s. deviation is approximately 0.75 Å, including a 0.76 Å deviation by V157F. The rescued cancer mutant (V157F/N235K/N239K) shows the highest r.m.s. deviation of 0.81 Å. When compared with the DNA-free wild-type p53 structure, the rescued cancer mutant also stands out with the largest r.m.s. deviation of 0.87 Å, whereas the cancer mutant V157F and the two suppressor mutants N235K and N239Y display significantly smaller deviations of 0.24, 0.23 and 0.20 Å, respectively (third column). Similar results are also found on the super-

position of other p53 structures (columns 4–6 and 8–13). In all cases, the largest r.m.s. deviation results from superposition of the rescued cancer mutant structure with either the DNA-free or DNA-bound p53 structures. Therefore, somewhat surprisingly, the largest structural changes are observed for the rescued cancer mutant and not, as one might naively have presumed, for the cancer mutant.

To identify specific regions of structural deviations in the rescued cancer mutant, we compared this structure with those of wild-type DNA-free p53 (PDB entry 2ocj, chain *B*) and DNA-bound p53 (PDB entry 1tsr, chain *B*) (Fig. 3*b*). The β-sandwich remains largely intact, with little backbone variability between the rescued cancer mutant and these two wild-type structures. The largest deviations occur in loops L1 and L2, both of which are located on the DNA-binding surface. The loop L1 structures of the rescued cancer mutant and both the DNA-free and DNA-bound wild-type p53 structures are mutually distinct. The largest deviation is at Ser121, for which the C^{α} atom of the rescued cancer mutant is displaced by 1.8 and 3.2 Å from the DNA-free and DNA-bound wild-type structures, respectively. Overall, the structure of loop L1 in the rescued cancer mutant is midway between those of the DNA-free and DNA-bound wild types, which themselves vary by 5.0 Å at Ser121, although it more closely resembles L1 of the DNA-free wild type. Although not involved in direct contacts with target DNA, loop L2 is near the DNA-binding surface. The C^{α} atom of Ser183 in loop L2 of the rescued cancer mutant is displaced 1.9 Å compared with the DNA-free structure and 3.1 Å compared with the DNA-bound structure. Again, loop L2 of the rescued cancer mutant is between that of the DNA-free and the DNA-bound loops, but more closely resembles that of the DNA-free wild type. Significant conformational changes are also detected in all turn regions opposite the DNA-binding surface, including turns S3/S4, S7/S8 and S9/S10.

3.3. Local structural changes at mutation sites

The V157F cancer mutation induces a significant local conformational change at Ile232, the C^{δ} and $C^{\gamma 1}$ atoms of which are displaced by a rotation around χ_1 (from the 60% rotamer with a χ_1 of -66° to the 2% rotamer with a χ_1 of -169°; Fig. 4) to accommodate the large hydrophobic benzyl moiety of Phe157. Surprisingly, this local repacking of the hydrophobic core results in only minor longer range structural changes, as indicated by the small r.m.s. deviation (0.24 Å) between the backbone-atom alignment of the V157F mutant compared with the DNA-free p53 structure. In contrast, the aromatic ring of Phe157 in the rescued cancer mutant is accommodated by significant structural changes in several neighboring residues (Fig. 4). Ile232 returns to a conformation similar to that observed in the wild type. The Tyr220 side chain is pushed away from the centre of the hydrophobic core, with its hydroxyl group displaced by 2.8 Å compared with the wild type. The side chain of Leu145 shows a more moderate rotation and shift. Additionally, Val218 and Tyr234 undergo conformational changes.

It is striking that the orientations of the phenyl group of Phe157 in the cancer mutant and the rescued cancer mutant are quite distinct, essentially projecting in opposite directions. In the V157F cancer mutant the phenyl group is oriented towards the interior of the hydrophobic core, where it is sandwiched between the side chains of Leu145 and Val218 (13% of a rotamer with a χ_1 of $+59^{\circ}$, although molecules *C* and *D* show partial occupancy for the 'rescued' rotamer as well), while in the rescued cancer mutant Phe157 points toward the edge of the β-sandwich, where it is sandwiched between Leu145 and Leu257 (44% of a rotamer with a χ_1 of -64°). Being buried within the hydrophobic core, the nearest ordered water molecule from wild-type Val157 is at a distance of 4.4 Å. In the V157F structure, the large phenylalanine protrudes across the β-sandwich through strands S7 and S8 towards the surrounding hydration shell. This protrusion causes the C^{ε} atom of Phe157 to come within 3.4 Å of an ordered water molecule. This solvent protrusion of Phe157 is only partially retained in the rescued cancer mutant structure; the C^{ε} atom is within 3.9 Å of an ordered water molecule, has the varied ring orientation and makes contact with a non-analogous water molecule.

In the wild-type p53 structure, a hydrogen bond exists between Asn235 in strand S8 and Glu198 in strand S5 on the solvated surface of the β-sandwich (Fig. 5*a*). However, in the N235K suppressor mutant the substituted Lys235 forms a 3.7 Å salt bridge with Glu198, which also contacts Thr140 in the turn between S2′ and S3 *via* a hydrogen bond. This

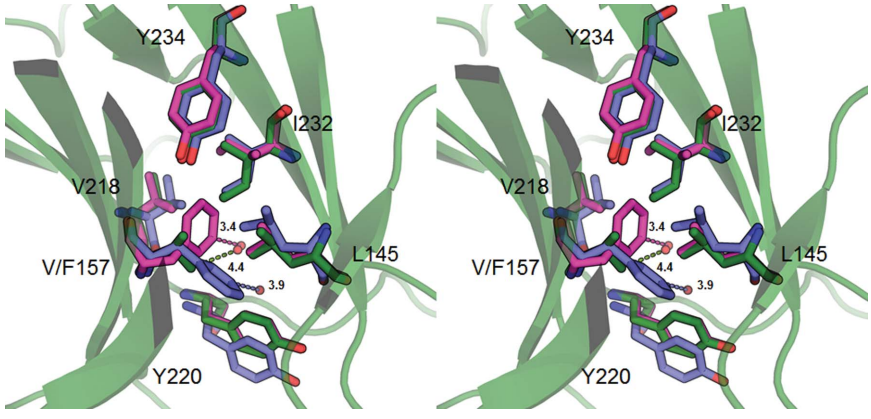

Figure 4
Structural effects of the cancer mutation V157F and its rescue. Stereoview of the mutation site with a backbone-atom alignment of the V157F cancer mutant (chain *B*; magenta), the rescued cancer mutant V157F/N235K/N239Y (blue) and the DNA-free wild-type p53 core domain (PDB entry 2ocj, chain *B*; green). A cartoon representation of the DNA-free wild-type p53 core-domain backbone is displayed for reference. Ordered water molecules are shown as red spheres with distances to protein atoms indicated by dashed lines of colour corresponding to the respective p53 variant.

network establishes a strong connection between S5 and S8 and the transition of the β-sandwich into the DNA-binding surface. A similar network of interactions occurs in the rescued cancer mutant. However, the salt-bridge distance between Lys235 and Glu198 is reduced to 2.9 Å in this structure and the Glu198–Thr140 hydrogen bond is lost. Taken together, these three amino acids in the N235K variant form a strong network between separate strands of the β-sandwich with Glu198 at its centre and this would be expected to contribute additional stability.

The second rescue mutation, Tyr239, is located in loop L3 on the DNA-binding surface and is exposed to the solvent in the crystal lattice. The C^{α} atom of Tyr239 is approximately 5 Å from the S atoms of two zinc-coordinating residues, Cys238 and Cys242, and only 5.3 Å away from the zinc ion itself. Meanwhile, Val274 and Cys275 in helix H2, which neighbor two important DNA-backbone contacts, Arg273 and Ala276, also lie in the Tyr239 region. In the N239Y structure, as well as in the thermostable mutant (T-p53), a novel hydrophobic contact is created between the aromatic ring of Tyr239 and Leu137 (Fig. 5*b*; Joerger *et al.*, 2004). In the wild-type structure, this leucine side chain appears to be predominantly exposed to solvent. Despite this novel hydrophobic contact in the N239Y structure, Leu137 remains in a relatively similar position compared with the wild type. However, in the rescued cancer mutant the side chain of Leu137 has shifted slightly towards Tyr239, with a C^{γ}–C^{ε} distance of 3.4 Å compared with 3.8 Å for N239Y alone. Extending into the solvent, the hydroxyl of the Tyr239 phenol moiety hydrogen-bonds to a nearby water molecule in all structures containing this mutation: N239Y, V157F/N235K/N239Y and the thermostable mutant. Other nearby amino acids undergo only slight conformational changes. Noticeably, the side chains of Tyr239 in these three structures are arranged in the same orientation, with slight shifts of the phenol groups. As also described by Joerger and coworkers, overlaying these DNA-free N239Y variants with DNA-bound p53 illustrates the proximity of Tyr239 to the DNA-binding interface, with the hydroxyl of the rescued cancer mutant approximately 3.5 Å from the DNA phosphodiester backbone (Joerger *et al.*, 2004).

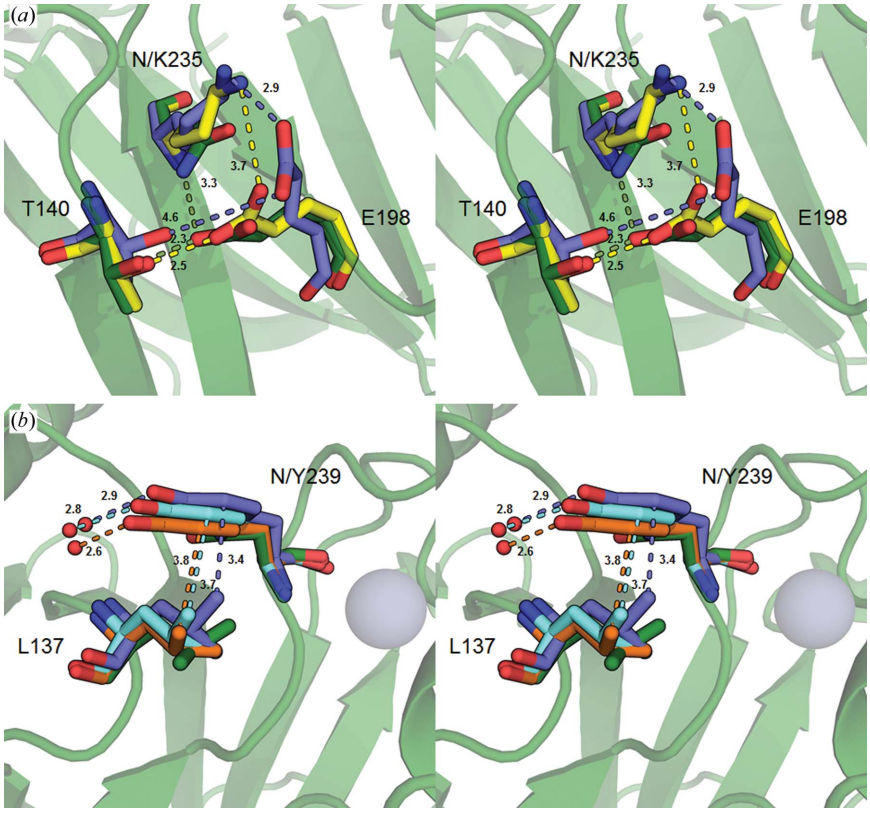

Figure 5
Local conformational changes at the sites of suppressor mutations. A comparison of different structures, the N235K mutant (chain *B*; yellow), the N239Y mutant (chain *B*; orange), the rescued cancer mutant V157F/N235K/N239Y (blue), the thermostable mutant (PDB entry 1uol, chain *B*; cyan) and DNA-free wild-type p53 (PDB entry 2ocj, chain *B*; green), is performed using backbone-atom superposition. A cartoon representation of the DNA-free wild-type p53 core-domain backbone is displayed for reference. (*a*) Stereoview of the mutation site N235K. The suppressor mutation N235K creates a novel salt bridge between Lys235 and Glu198. Distances for salt bridges and hydrogen bonds are indicated by dashed lines of colour corresponding to the respective p53 variant. (*b*) Stereoview of the N239Y mutation site. The suppressor mutation N239Y generates a hydrophobic contact with Leu137 and hydrogen bonds to solvent water molecules. Interatomic distances between Tyr239 and Leu137 and ordered water molecules are indicated by dashed lines of colour corresponding to the respective p53 variant.

4. Discussion

Here, we present biochemical and structural studies of V157F, an oncogenic p53 mutation occurring in the β-sandwich of the core domain, both with and without the associated second-site rescue mutations N235K and N239Y. This is the first structure of a β-sandwich cancer mutant without additional stabilizing mutations. To understand the structural effects of these deleterious mutations, particularly for those mutations expected to lead to structural and thermodynamic abnormalities, it is meaningful to study them without added stabilizing or rescue mutations which could potentially mask their actual effects. This is especially important since there is only a crystal structure of one other core-domain missense mutant, R249S, a local structure-perturbing mutant, which does not contain stabilizing mutations (Suad *et al.*, 2009; Bullock *et al.*, 2000). The mechanism of rescue by these two suppressor mutations, N235K, a novel mutation, and N239Y, which has been studied in the context of T-p53, are also considered.

4.1. Destabilizing mechanism of V157F mutation

Statistical analysis reveals that the mutation frequency of p53 at codon 157 repre-

sents about 1% of point mutations, where V157F contributes to 77% of missense mutations at this codon (Petitjean *et al.*, 2007). Denaturation studies show that the V157F mutation destabilizes the core domain by 3.6 kcal mol^{-1} and disturbances in the hydrophobic packing of the β-sandwich are visible based on the crystal structure (Fig. 4). The induced steric clashes in the core, which cause the rearrangement of several surrounding side chains and reduced shielding from the solvent, are likely to account for this loss in stability. However, only minor deviations of the protein backbone, both in this region and in the overall domain, are observed.

The crystal structures of two other deleterious mutations within the hydrophobic core, V143A (PDB entry 2j1w) and F270L (PDB entry 2j1z), have been solved on the background of the thermostable p53 mutant (M133L, V203A, N239Y and N268D; Joerger *et al.*, 2006). These mutations have the opposite substitution effects as V157F, as both are large-to-small mutations within the core. Both V143A and F270L create an internal cavity within the hydrophobic core. All three of these hydrophobic side-chain substitutions cause similar destabilizing effects on the core domain: a 3.5–4.5 kJ mol^{-1} loss in stability (Bullock *et al.*, 2000). This indicates that the β-sandwich contains a fairly stringent organization, in which increases or decreases in the mass of side chains of a single side chain, even if the substitution preserves the hydrophobicity of the core, are not well tolerated.

4.2. Structural effects of rescue mutations N235K and N239Y

Structural studies reveal the mechanism of rescue for two suppressor mutations, N235K and N239Y, which are particularly effective at rescuing β-sandwich mutations both alone and in concert. The novel N235K mutation structure presents a new salt bridge on the surface of the β-sandwich between strands S8 and S5. This additional salt bridge is able to restabilize the V157F mutant by 1.3 kcal mol^{-1}, although little stabilization is gained when this salt bridge is added to the wild-type core domain. This is likely to be because the V157F mutation disrupts the packing of the hydrophobic core and the added salt bridge is able to overcome any loss in stability of this core. The V157F mutation causes the most drastic rearrangement of the Ile232 side chain, which is located on S8, the same β-strand that contains Lys235 and the new salt bridge in the rescued mutant. It appears that addition of the Lys235–Glu198 interaction is able to compensate for the unfavorable packing of the β-sandwich by fastening these two β-strands together. N235K shows no stability gain when added to the wild-type core domain, which does not have an unfavorable packing of its hydrophobic core. The effects of the Lys235–Glu198 interaction salt bridge may only be apparent in variants with perturbations of the β-sandwich. The N235K suppressor mutation was originally discovered for its ability to rescue cancer mutations in combination with other second-site suppressor mutations, mostly in codons 239 and 240, based on functional p53 yeast assays (Baroni *et al.*, 2004). These combination suppressor mutations were able to recover the function of deleterious mutations in the β-sandwich, as well as in other areas of the core domain. Although N235K demonstrates an ability to stabilize the V157F mutation here, it is difficult to discern whether this rescue mutation has utility against mutations outside of β-sandwich destabilization.

The N239Y suppressor mutation demonstrates the capacity to add stability, approximately 1 kcal mol^{-1}, to either the wild type or the V157F/N235K mutant. Utilizing the structure of this N239Y mutation, the aromatic ring of Tyr239 makes a unique hydrophobic contact with Leu137 and its hydroxyl moiety extends to hydrogen bond with the solvent. As Leu137 is normally solvent-exposed, a majority of the reduction in free energy caused by this substitution can be attributed to a gain in entropy at the protein–solvent surface, with the phenol group both protecting this leucine from solvent as well as allowing hydrogen bonding with the surrounding water. Comparing the N239Y, rescued cancer mutant and thermostable mutant structures, the orientation of the Tyr239 phenol moiety is very similar and a consistent distance is observed between it and Leu137, indicating a conserved mechanism of N239Y rescue. Also, Tyr239 lies at the DNA-binding interface of the core domain and may be able to make favorable interactions with the phosphodiester backbone of the DNA. In particular, N239Y acts as a rescue mutation at a very distant site from the original deleterious mutation V157F. With the ability to add stability to the core domain as well as rescue the function of several cancer-causing mutations, N239Y is likely to act as a global second-site suppressor mutation (Baroni *et al.*, 2004; Brachmann, 2004). This means that the gain in stability from Tyr239 may be able to compensate for a wide variety of deleterious mutations: stability mutations and local structural deviations alike.

Surprisingly, the overall fold of the wild-type structure aligns more closely with that of the destabilized cancer mutant V157F than that of the rescued cancer mutant V157F/N235K/N239Y. This seems to indicate that the two suppressor mutations presented here do not function by simply reversing the effects of the deleterious mutation and returning the structure of the protein to a more native-like fold. Instead, their introduction seems to create novel molecular interactions which enhance the overall stability of the protein, allowing it to retain function within the cell.

4.3. Beyond second-site suppressor mutations

One goal of the field is to identify pharmaceuticals that can restore wild-type function to p53 mutants. Over the past decade, a variety of cell-based screening techniques have led to the discovery of several small molecules which appear to rescue the function of mutant p53 (Foster *et al.*, 1999; Bykov *et al.*, 2002; Yu *et al.*, 2012). One of these small molecules, APR-246 (PRIMA-1MET), is currently in Phase I/II clinical trials (Lehmann *et al.*, 2012). Despite these advances, the actual binding of these small molecules to p53 and their mechanisms of rescue have remained elusive. This lack of understanding has hampered the development of small molecules into useful pharmaceuticals in the clinic. The structures of second-site

suppressor mutations are giving us the tools to understand mechanisms of counteracting oncogenic mutations in the core domain of p53. By understanding how some of these rescue mutations function, particularly global suppressor mutations such as N239Y, we are beginning to understand how a pharmaceutical could function in this capacity. Recently, the understanding of these second-site suppressors has helped to guide the discovery of a pocket within the core domain which could be targeted for pharmaceutical rescue (Wassman *et al.*, 2013). Subsequent *in silico* screening of this pocket identified a small molecule which stabilizes the core domain of mutant p53 and allows it to regain wild-type transcriptional activity (Wassman *et al.*, 2013).

We thank Dr Rainer Brachmann for generously providing the expression plasmids for all four p53 core-domain mutants. We also thank Drs Rainer Brachmann and Melanie Cocco for discussions. We thank Dr Lihua Tan for pointing out the possibility of merohedral twinning of the V157F data set. This research was supported by NIH grant R01-GM067808 (HL), by NSF grants MCB-0215769 and MCB-0719373 (DS) and by a UCI Chancellor's Fellowship (HL). Ikerbasque is thanked for a part-time Research Professorship.

References

Adams, P. D. *et al.* (2010). *Acta Cryst.* D**66**, 213–221.
Afonine, P. V., Grosse-Kunstleve, R. W., Echols, N., Headd, J. J., Moriarty, N. W., Mustyakimov, M., Terwilliger, T. C., Urzhumtsev, A., Zwart, P. H. & Adams, P. D. (2012). *Acta Cryst.* D**68**, 352–367.
Aramayo, R., Sherman, M. B., Brownless, K., Lurz, R., Okorokov, A. L. & Orlova, E. V. (2011). *Nucleic Acids Res.* **39**, 8960–8971.
Baroni, T. E., Wang, T., Qian, H., Dearth, L. R., Truong, L. N., Zeng, J., Denes, A. E., Chen, S. W. & Brachmann, R. K. (2004). *Proc. Natl Acad. Sci. USA*, **101**, 4930–4935.
Brachmann, R. K. (2004). *Cell Cycle*, **3**, 1030–1034.
Brachmann, R. K., Yu, K., Eby, Y., Pavletich, N. P. & Boeke, J. D. (1998). *EMBO J.* **17**, 1847–1859.
Brünger, A. T., Adams, P. D., Clore, G. M., DeLano, W. L., Gros, P., Grosse-Kunstleve, R. W., Jiang, J.-S., Kuszewski, J., Nilges, M., Pannu, N. S., Read, R. J., Rice, L. M., Simonson, T. & Warren, G. L. (1998). *Acta Cryst.* D**54**, 905–921.
Bullock, A. N. & Fersht, A. R. (2001). *Nature Rev. Cancer*, **1**, 68–76.
Bullock, A. N., Henckel, J., DeDecker, B. S., Johnson, C. M., Nikolova, P. V., Proctor, M. R., Lane, D. P. & Fersht, A. R. (1997). *Proc. Natl Acad. Sci. USA*, **94**, 14338–14342.
Bullock, A. N., Henckel, J. & Fersht, A. R. (2000). *Oncogene*, **19**, 1245–1256.
Bykov, V. J., Issaeva, N., Shilov, A., Hultcrantz, M., Pugacheva, E., Chumakov, P., Bergman, J., Wiman, K. G. & Selivanova, G. (2002). *Nature Med.* **8**, 282–288.
Chen, V. B., Arendall, W. B., Headd, J. J., Keedy, D. A., Immormino, R. M., Kapral, G. J., Murray, L. W., Richardson, J. S. & Richardson, D. C. (2010). *Acta Cryst.* D**66**, 12–21.
Cho, Y., Gorina, S., Jeffrey, P. D. & Pavletich, N. P. (1994). *Science*, **265**, 346–355.
Danziger, S. A., Zeng, J., Wang, Y., Brachmann, R. K. & Lathrop, R. H. (2007). *Bioinformatics*, **23**, i104–i114.
DeLano, W. L. (2002). *PyMOL*. http://www.pymol.org.
Emsley, P. & Cowtan, K. (2004). *Acta Cryst.* D**60**, 2126–2132.
Evans, P. (2006). *Acta Cryst.* D**62**, 72–82.
Foster, B. A., Coffey, H. A., Morin, M. J. & Rastinejad, F. (1999). *Science*, **286**, 2507–2510.
Joerger, A. C., Allen, M. D. & Fersht, A. R. (2004). *J. Biol. Chem.* **279**, 1291–1296.
Joerger, A. C., Ang, H. C. & Fersht, A. R. (2006). *Proc. Natl Acad. Sci. USA*, **103**, 15056–15061.
Joerger, A. C., Ang, H. C., Veprintsev, D. B., Blair, C. M. & Fersht, A. R. (2005). *J. Biol. Chem.* **280**, 16030–16037.
Joerger, A. C. & Fersht, A. R. (2008). *Annu. Rev. Biochem.* **77**, 557–582.
Jones, T. A., Zou, J.-Y., Cowan, S. W. & Kjeldgaard, M. (1991). *Acta Cryst.* A**47**, 110–119.
Krissinel, E. & Henrick, K. (2004). *Acta Cryst.* D**60**, 2256–2268.
Kruse, J. P. & Gu, W. (2009). *Cell*, **137**, 609–622.
Laskowski, R. A., Rullmannn, J. A., MacArthur, M. W., Kaptein, R. & Thornton, J. M. (1996). *J. Biomol. NMR*, **8**, 477–486.
Lehmann, S., Bykov, V. J., Ali, D., Andren, O., Cherif, H., Tidefelt, U., Uggla, B., Yachnin, J., Juliusson, G., Moshfegh, A., Paul, C., Wiman, K. G. & Andersson, P. O. (2012). *J. Clin. Oncol.* **30**, 3633–3639.
McLure, K. G. & Lee, P. W. K. (1998). *EMBO J.* **17**, 3342–3350.
Melero, R., Rajagopalan, S., Lázaro, M., Joerger, A. C., Brandt, T., Veprintsev, D. B., Lasso, G., Gil, D., Scheres, S. H. W., Carazo, J. M., Fersht, A. R. & Valle, M. (2011). *Proc. Natl Acad. Sci. USA*, **108**, 557–562.
Nikolova, P. V., Henckel, J., Lane, D. P. & Fersht, A. R. (1998). *Proc. Natl Acad. Sci. USA*, **95**, 14675–14680.
Nikolova, P. V., Wong, K.-B., DeDecker, B., Henckel, J. & Fersht, A. R. (2000). *EMBO J.* **19**, 370–378.
Pace, C. N. (1986). *Methods Enzymol.* **131**, 266–280.
Petitjean, A., Mathe, E., Kato, S., Ishioka, C., Tavtigian, S. V., Hainaut, P. & Olivier, M. (2007). *Hum. Mutat.* **28**, 622–629.
Pflugrath, J. W. (1999). *Acta Cryst.* D**55**, 1718–1725.
Riley, T., Sontag, E., Chen, P. & Levine, A. (2008). *Nature Rev. Mol. Cell Biol.* **9**, 402–412.
Rippin, T. M., Freund, S. M., Veprintsev, D. B. & Fersht, A. R. (2002). *J. Mol. Biol.* **319**, 351–358.
Römer, L., Klein, C., Dehner, A., Kessler, H. & Buchner, J. (2006). *Angew. Chem. Int. Ed. Engl.* **45**, 6440–6460.
Senear, D. F. & Brenowitz, M. (1991). *J. Biol. Chem.* **266**, 13661–13671.
Storoni, L. C., McCoy, A. J. & Read, R. J. (2004). *Acta Cryst.* D**60**, 432–438.
Suad, O., Rozenberg, H., Brosh, R., Diskin-Posner, Y., Kessler, N., Shimon, L. J. W., Frolow, F., Liran, A., Rotter, V. & Shakked, Z. (2009). *J. Mol. Biol.* **385**, 249–265.
Tretyachenko-Ladokhina, V., Cocco, M. J. & Senear, D. F. (2006). *J. Mol. Biol.* **362**, 271–286.
Vogelstein, B., Lane, D. & Levine, A. J. (2000). *Nature (London)*, **408**, 307–310.
Vousden, K. H. & Lu, X. (2002). *Nature Rev. Cancer*, **2**, 594–604.
Wang, W., Rastinejad, F. & El-Deiry, W. S. (2003). *Cancer Biol. Ther.* **2**, S55–S63.
Wang, Y., Rosengarth, A. & Luecke, H. (2007). *Acta Cryst.* D**63**, 276–281.
Wassman, C. D., Baronio, R., Demir, Ö., Wallentine, B. D., Chen, C.-K., Hall, L. V., Salehi, F., Lin, D.-W., Chung, B. P., Hatfield, G. W., Chamberlin, A. R., Luecke, H., Lathrop, R. H., Kaiser, P. & Amaro, R. E. (2013). *Nature Commun.* **4**, 1407.
Weinberg, R. L., Veprintsev, D. B. & Fersht, A. R. (2004). *J. Mol. Biol.* **341**, 1145–1159.
Wieczorek, A. M., Waterman, J. L., Waterman, M. J. & Halazonetis, T. D. (1996). *Nature Med.* **2**, 1143–1146.
Yu, X., Vazquez, A., Levine, A. J. & Carpizo, D. R. (2012). *Cancer Cell*, **21**, 614–625.